JOURNAL OF GEOPHYSICAL RESEARCH, VOL. 113, D21122, doi:10.1029/2008JD009817, 2008

An improved comparison of atmospheric Ar/N_2 time series and paired ocean-atmosphere model predictions

Nicolas Cassar,[1] Galen A. McKinley,[2] Michael L. Bender,[1] Robert Mika,[1] and Mark Battle[3]

Received 11 January 2008; revised 21 July 2008; accepted 28 August 2008; published 15 November 2008.

[1] Ar/N_2 variations in the atmosphere reflect ocean heat fluxes, air-sea gas exchange, and atmospheric dynamics. Here atmospheric Ar/N_2 time series are compared to paired ocean-atmosphere model predictions. Agreement between Ar/N_2 observations and simulations has improved in comparison to a previous study because of longer time series and the introduction of automated samplers at several of the atmospheric stations, as well as the refinement of the paired ocean-atmosphere models by inclusion of Ar and N_2 as active tracers in the ocean component. Although analytical uncertainties and collection artifacts are likely to be mainly responsible for observed Ar/N_2 outliers, air parcel back-trajectory analysis suggests that some of the variability in Ar/N_2 measurements could be due to the low-altitude history of the air mass collected and, by extension, the local oceanic Ar/N_2 signal. Although the simulated climatological seasonal cycle can currently be evaluated with Ar/N_2 observations, longer time series and additional improvements in the signal-to-noise ratio will be required to test other model predictions such as interannual variability, latitudinal gradients, and the secular increase in atmospheric Ar/N_2 expected to result from ocean warming.

Citation: Cassar, N., G. A. McKinley, M. L. Bender, R. Mika, and M. Battle (2008), An improved comparison of atmospheric Ar/N_2 time series and paired ocean-atmosphere model predictions, *J. Geophys. Res.*, *113*, D21122, doi:10.1029/2008JD009817.

1. Introduction

[2] The atmospheric ratio of argon to nitrogen (Ar/N_2) varies seasonally because, in part, solubilities of these gases change with temperature. Since Ar is approximately twice as soluble as N_2, the atmospheric Ar/N_2 ratio increases as the surface oceans warm (i.e., spring, summer) and degas. The opposite occurs during cooling (i.e., fall, winter). At a given atmospheric sampling site, the Ar/N_2 seasonal amplitude is a function of the oceanic temperature change, the air-sea gas exchange rate, and the dilution of the Ar/N_2 signal by atmospheric transport and mixing [*Battle et al.*, 2003; *Keeling et al.*, 2004]. In this respect, atmospheric Ar/N_2 is a valuable tracer of the complex interplay of upper ocean heating, air-sea gas flux kinetics, and atmospheric transport dynamics. Temporal (e.g., interannual) variability in these processes should be reflected in the atmospheric Ar/N_2 record, and differences between sampling sites may highlight spatial variations in these processes. Furthermore, the rise in sea surface ocean temperature [*Levitus et al.*, 2005, 2000] should manifest itself as a secular increase in the Ar/N_2 ratio in air.

[3] Comparing Ar/N_2 observations with simulations from paired ocean-atmosphere models tests the robustness of simulations of upper ocean mixing, air-sea heat fluxes and atmospheric transport. *Battle et al.* [2003] observed significant differences in the amplitude and phasing of observations and models. These differences were attributed to sampling artifacts, the assumption in the models of instantaneous equilibration of gases as the upper ocean gained or lost heat, and errors in the atmospheric transport simulation. Assuming instantaneous gas exchange caused the models' predictions to generally lead observations. The observed amplitudes of the annual Ar/N_2 cycle were comparable with model predictions, although observed amplitudes were generally larger than their modeled counterparts.

[4] Here, we present an updated time series which is approximately twice as long as the one presented by *Battle et al.* [2003]. In addition, a significant portion of the Ar/N_2 samples have now been collected with automated samplers at several collection sites, ameliorating collection artifacts and improving accuracy. We present new monthly Ar/N_2 climatologies and compare the results to paired ocean and atmospheric chemical transport model simulations that include Ar and N_2 as active tracers; that is, the ocean models now invoke kinetics of gas exchange rather than assuming instantaneous equilibration. On the basis of these improvements (i.e., longer time series, increased reproducibility in sample collection, and improved modeling of ocean-atmosphere gas exchange) a stronger correlation

[1]Department of Geosciences, Princeton University, Princeton, New Jersey, USA.
[2]Department of Atmospheric and Oceanic Sciences, University of Wisconsin-Madison, Madison, Wisconsin, USA.
[3]Department of Physics and Astronomy, Bowdoin College, Brunswick, Maine, USA.

0148-0227/08/2008JD009817$09.00

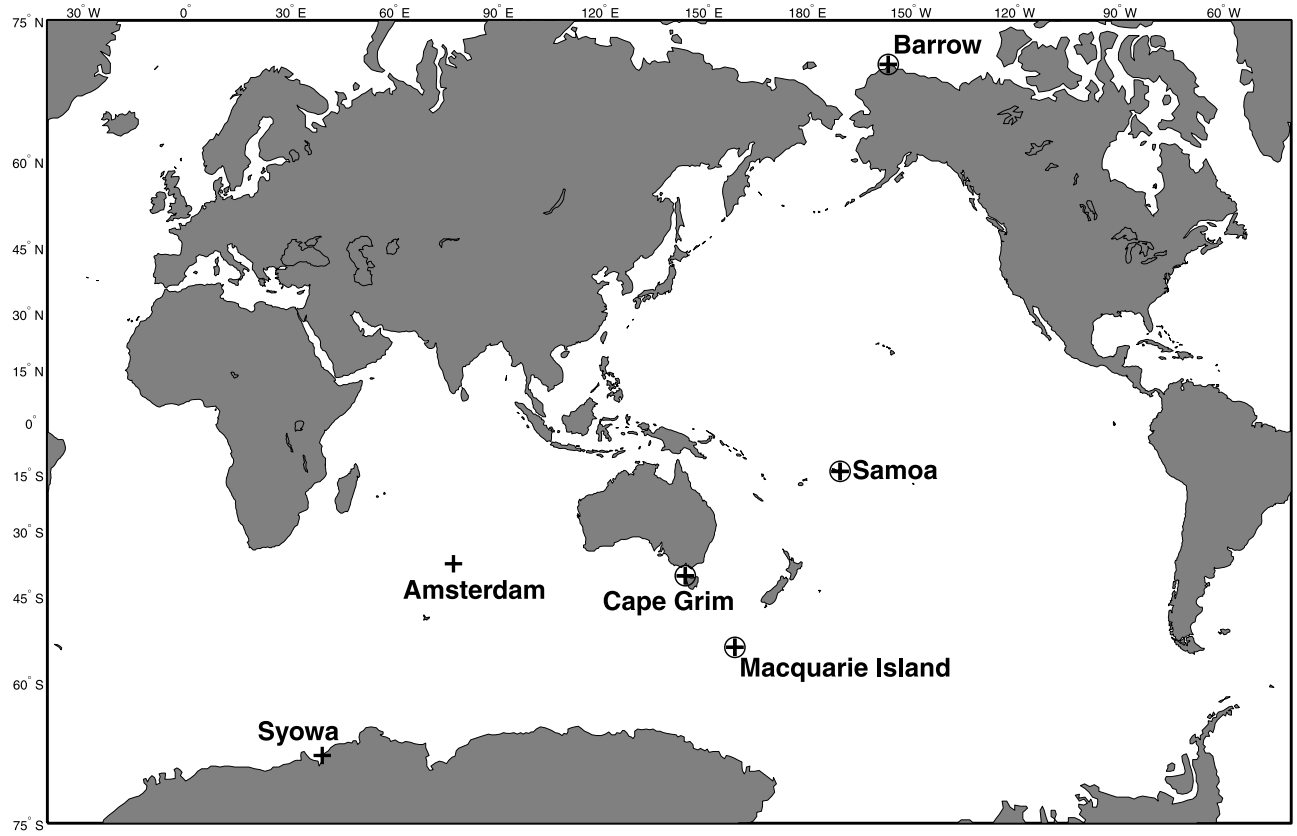

Figure 1. Atmospheric Ar/N_2 stations: Syowa (SYO), Amsterdam Island (AMS), Cape Grim (CGT), Macquarie Island (MAC), Samoa (SMO), and Barrow (BRW). Circled crosses represent stations where automated samplers are present.

between model predictions and observations is observed. Air parcel back trajectory analyses were also performed to explore stations differences in atmospheric Ar/N_2.

2. Material and Methods

2.1. Measurements of Atmospheric Ar/N_2

[5] Sample collection, measurements and corrections are made as described in the auxiliary online material of *Battle et al.* [2003] and for O_2/N_2 ratios by *Bender et al.* [2005]. Briefly, duplicate air samples were collected in 2-L bottles at 6 sites (Figure 1) weekly or semimonthly starting in 1999, and assayed for Ar/N_2 and O_2/N_2. Between 2002 and 2005, automated air samplers, with a design similar to the one presented by *Neubert et al.* [2004], were installed at four of our six sampling sites: Cape Grim, Barrow, Samoa, and Macquarie Island. Automated samplers were installed to reduce potential collection artifacts and further standardize sample collection between stations. During automated sampling, air is pumped through a cryogenic moisture trap, and directed to one of the duplicate sample bottles (Figure 2). Automated sampling involved higher flow rates of air, better cryotrapping of water, and standardization of the collection procedure.

[6] Samples from manual and automated sampling were later analyzed in Princeton on a Finnigan Delta isotope-ratio mass spectrometer with a customized dual inlet [*Battle et al.*, 2003; *Bender et al.*, 2005]. Analysis errors have been thoroughly discussed by *Battle et al.* [2003]. As in work by *Battle et al.* [2003], Ar/N_2 measurements are reported relative to a laboratory standard in units of per meg,

$$\delta(Ar/N_2) = [\frac{(Ar/N_2)_{SA}}{(Ar/N_2)_{ST}} - 1] \times 10^6,$$

where the subscripts "SA" and "ST" stand for sample and standard, respectively. An integrated data system based on Matlab and FileMakerPro software performs the corrections described for O_2/N_2 ratios by *Bender et al.* [2005].

[7] Outliers were identified by visual inspection followed by an iterative removal of observations more than 3 sigma from a smooth curve fit based on a robust locally weighted scatterplot (LOESS) with a span parameter of 30 points (approximately 1.25 years) [*Cleveland*, 1979; *Cleveland and Devlin*, 1988]. On the basis of the visual inspection and the iterative process, 9 or fewer observations per station were removed (approximately 4% of all samples analyzed). All analyses and climatologies are based on the time series with outliers excluded.

2.2. Paired Atmosphere-Ocean Models

[8] The ocean models used are variants of the Modular Ocean Model, version 4 (MOM4), part of the Geophysical Fluid Dynamics Laboratory (GFDL) Flexible Modeling System. We used two versions of this model. MOM4 OM1 [*Griffies et al.*, 2004] is a coarser resolution version,

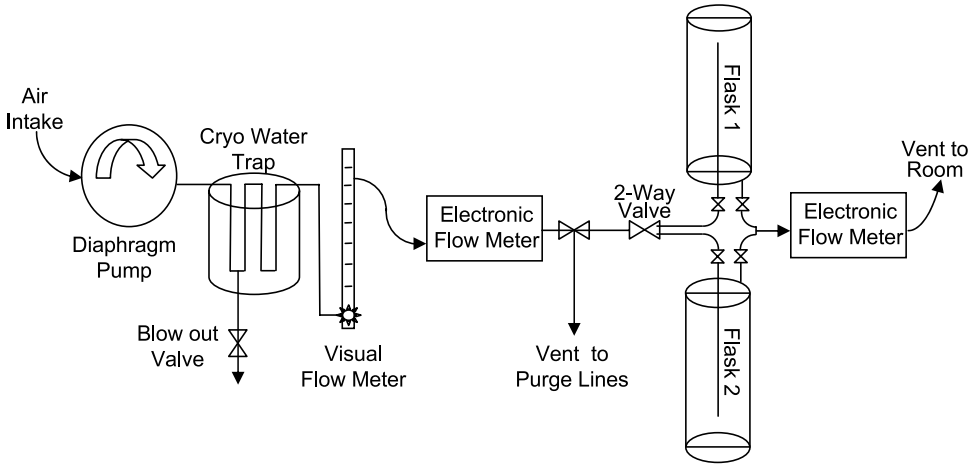

Figure 2. Schematic of automated sampling unit used at Cape Grim, Barrow, Macquarie, and Samoa atmospheric stations.

at 4.5° × 3.75° and 24 vertical levels, 25 m in the first two layers. Background horizontal diffusion is 1000 $cm^2\ s^{-1}$ and background vertical diffusion is 0.3 $cm^2\ s^{-1}$. Shortwave radiation does not penetrate beyond the first model layer. MOM4 OM1p5 [*Griffies et al.*, 2004] has increased horizontal and vertical resolution, at 3.0° × 0.6–3.0° and 28 vertical levels, with 10m vertical spacing from 0 to 80m. Background horizontal diffusion is 600 $cm^2\ s^{-1}$ and background vertical diffusion is 0.45 $cm^2\ s^{-1}$. OM1p5 includes penetration of shortwave radiation up to 150m depth as a function of climatologically observed chlorophyll. In both OM1 and OM1p5, air-sea gas exchange is calculated following *Wanninkhof* [1992], and the OCMIP2 [*Orr et al.*, 2001] sea ice climatology is applied to inhibit air-sea gas transfer. The models do not account for the effect of supersaturation due to bubble injection. The ocean models are forced with climatological wind stress and heat fluxes from the NCEP/NCAR Reanalysis [*Kalnay et al.*, 1996]. The physical models were both spun up from rest for several hundred years before tracers were introduced. Tracers were run for 1100 years before results were analyzed.

[9] The general circulation patterns of both OM1 and OM1p5 are reasonable for coarse resolution ocean general circulation models. The model versions give North Atlantic Deep Water (NADW) formation rates of 15–17 Sv, consistent with *Ganachaud and Wunsch* [2000]. They give Antarctic Bottom Water (AABW) formation rates of 5–10 Sv, which is somewhat low [*Ganachaud and Wunsch*, 2000]. *McKinley* [2004] evaluated the mixed layer depths and thermocline structures of both models in comparison to climatological data. Both models perform reasonably well overall, with OM1p5 being a somewhat better simulation, as expected given its increased horizontal and vertical resolution. We compared the OM1 and OM1p5 results to profiles of Ar and N_2 in the ocean (auxiliary material Figure S1).[1] We find that the lack of the bubble effect in the air-sea gas exchange parameterization is a deficiency, causing greater underestimation of the ocean uptake of N_2 than of Ar. However, seasonal changes in solubility overwhelm seasonal changes in bubble injection in the surface ocean. For comparison, we also calculate air-sea Ar and N_2 fluxes based simply on OM1 and OM1p5 heat fluxes (hereafter defined as OM1HF and OM1p5HF, respectively), as performed by *Battle et al.* [2003]. These gas fluxes correspond to instantaneous air-sea equilibration, or infinitely large gas exchange coefficients.

[10] For atmospheric transport calculations, monthly mean air-sea Ar and N_2 fluxes from the ocean are circulated using the Global Chemical Transport Model (GCTM) [*Fan et al.*, 2004; *Mahlman and Moxim*, 1978], with an equal area grid (~265 km) and 28 sigma levels. NCEP/NCAR reanalyzed winds from 1995 to 2003 drive the tracer transport. Monthly mean Ar/N_2 ratios at the latitude, longitude and height of each station for 1999–2003 are averaged to a climatological seasonal cycle for comparison to data.

3. Results and Discussion

[11] With the ocean warming [*Levitus et al.*, 2005, 2000], the Ar/N_2 ratio of air is predicted to rise. However, our measurements are not precise enough (Figure 3) to observe the small changes in the atmosphere that are predicted, on the order of 2 per meg, over the length of the record [*Battle et al.*, 2003; *Keeling et al.*, 2004].

[12] Consistent with this limitation, our data show no significant temporal trend in Ar/N_2 ratios. To test for such a trend, we removed the median Ar/N_2 value for each site from all data for that site. We then stacked records from all sites and regressed Ar/N_2 versus sampling date. The slope of the median normalized Ar/N_2 observations for all stations is not significantly different from zero (slope = −0.017 per meg a^{-1}, standard error = 0.16, Degrees of Freedom = 1314, p = 0.91). This is evidence that there is little drift in the Ar/N_2 measurements of the laboratory standards, but also that we are currently unable to detect the expected secular increase in atmospheric Ar/N_2 due to warming of the surface oceans. Even if we did observe the expected trend, we could not rule out at this point the

[1] Auxiliary materials are available in the HTML. doi:10.1029/2008JD009817.

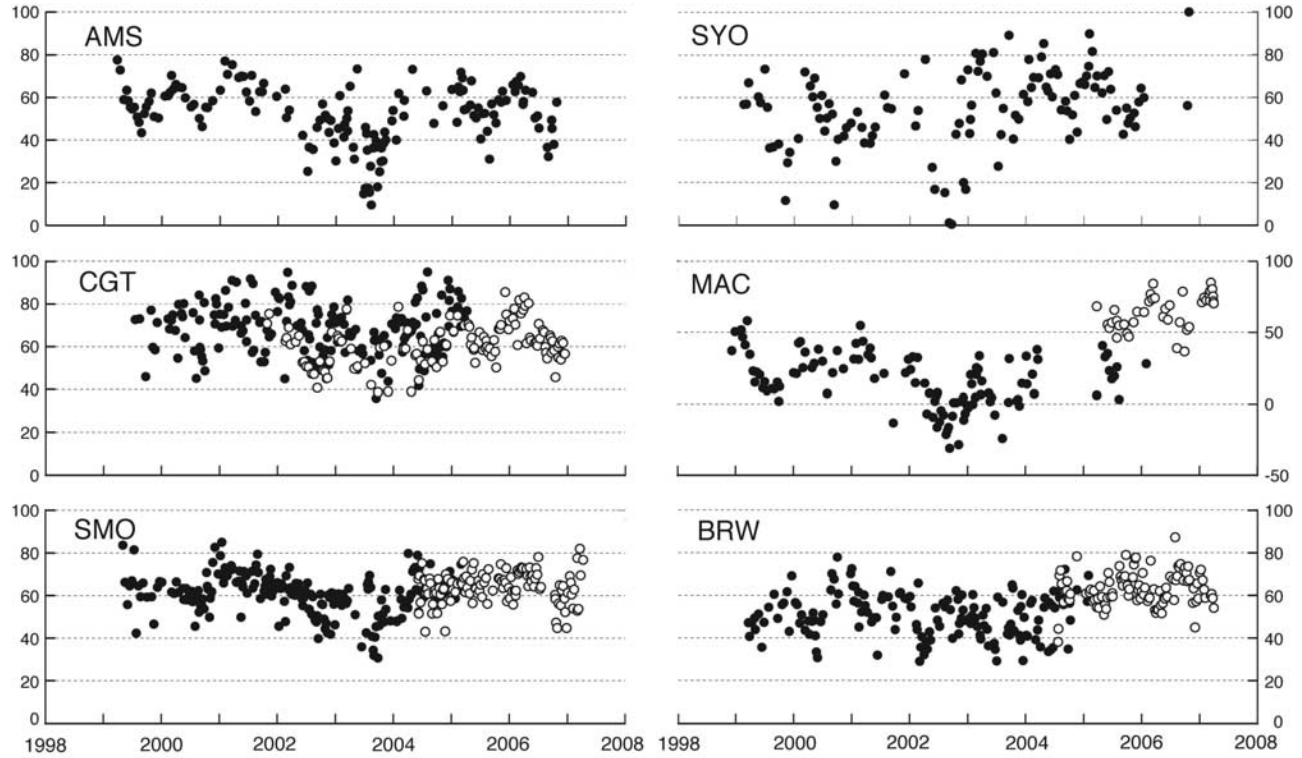

Figure 3. All Ar/N_2 observations (i.e., including outliers) by manual (solid circles) and automated (open circles) sampling at the various stations.

possibility that agreement resulted from a fortuitous drift in our standard curve.

3.1. Collection Artifacts Associated With Manual and Automated Sampling

[13] Judged by several criteria, automated sampling has greatly reduced collection artifacts. The simplest test is to compare the standard deviations of all samples (including outliers) measured with each of the two collection methods at a given site. Atmospheric variability contributes to the standard deviation, but lower values for automated samples reflect greater collection artifacts associated with the manual method (Table 1). A two-tailed F-test confirms that the differences in variance between automated and manual sampling are statistically significant (Table 1). On the basis of the standard deviation analysis, it is obvious that Macquarie Island in particular was plagued by collection artifacts which have greatly decreased with the introduction of automated sampling (Table 1). At Macquarie, the improved signal could also be due to the replacement of a t-junction line with a dedicated line when the automated sampler was installed. Fractionation in gas ratios at junctions has been reported in previous studies [*Manning*, 2001; *Stephens et al.*, 2007]. The automated samplers have also substantially increased the reproducibility between duplicate bottles (Table 1). Except at Cape Grim, the percent of duplicates that differ by more than 16 per meg is substantially smaller for automated relative to manual sampling (Table 1).

[14] On the basis of model predictions (see below), the difference in annual mean Ar/N_2 between stations is expected to be around 2 per meg or less [*Battle et al.*, 2003]. This number reflects rectifier effects as well as atmospheric transport from ocean regions where seawater is warming to regions of cooling. Greater variability is attributable to systematic artifacts in sample collection. On the basis of the standard deviation among the means of the stations (Table 1), we observe that the variance in the mean annual Ar/N_2 ratios is much smaller at the 4 stations with automated sampling (BRW, CGT, MAC, SMO) than with manual sampling at the same stations. *Battle et al.* [2003] reported a standard deviation of 19 per meg for these stations with manual sampling. We report for these same stations standard deviations of 23 and 1.7 per meg for manual and automated sampling, respectively. Although the change in the annual mean Ar/N_2 at Macquarie Island is responsible for most of this improvement, the decrease in standard deviation is also significant when Macquarie is excluded from the analysis (8.5 and 1.5 per meg standard deviation for manual and automated samplers, respectively). If we take the annual mean of the four stations with automated samplers, models predict that BRW, SMO, CGT and MAC are −0.5, 0.0, 0.1 and 0.4 per meg from the mean. Our observations at the same stations diverge from the mean by −0.3, 0.8, −2.2, and 1.8 per meg, respectively. Overall, the improved observations with automated samplers confirm that some of the variability is in fact attributable to collection artifacts, and that collection artifacts are diminished with automated sampling.

[15] The introduction of automated samplers also decreases the seasonal amplitude at all the stations (Table 1), which may reflect the lower seasonal variations in thermal fractionation at the air intake with automated versus manual sampling,

Table 1. Sampling Sites and Summary of Results From This Study[a]

	Barrow, Alaska (BRW) 71°19′N 156°36′W	American Samoa (SMO) 14°14′S 170°34′W	Amsterdam Island (AMS) 37°55′S 77°32′E	Cape Grim, Tasmania (CGT) 40°41′S 144°41′E	Macquarie Island (MAC) 54°30′S 158°57′E	Syowa, Antarctica (SYO) 69°00′S 39°35′E
			Duration and (Number) of Ar/N_2 Observations			
Manual	03/99–01/05 (156)	04/99–04/05 (213)	03/99–10/06 (150)	07/99–04/05 (183)	12/98–02/06 (112)	02/99–10/06 (119)
Automated	07/04–03/07 (103)	06/04–04/07 (119)	NA	10/01–12/06 (120)	03/05–04/07 (41)	NA
			Mean and (Standard Deviation) of Ar/N_2 Measurements (per meg)			
Manual	51 (10.3)	61 (9.4)	52 (13.8)	68 (11.8)	16 (19.0)	55 (18.3)
Automated	63 (7.9)	64 (7.4)	NA	61 (9.7)	65 (12.1)	NA
F-Test Probability	0.005	0.004	NA	0.023	0.002	NA
$\sigma^2_{Manual}/\sigma^2_{Automated}$ Confidence Interval	1.2–2.4	1.2–2.2	NA	1.1–2.0	1.4–4.0	NA
			Duplicate Bottle Agreement and (Median of Duplicate Standard Deviation)[b]			
Manual	5.8 (6.2)	9.9 (5.0)	8.0 (5.7)	6.5 (4.9)	8.8 (6.6)	12.1 (7.5)
Automated	2.6 (5.3)	2.2 (3.9)	NA	8.0 (4.7)	6.4 (5.6)	NA
			Seasonal Cycle Amplitude (per meg)			
Manual	18 ± 3	10 ± 3	21 ± 3	15 ± 3	34 ± 8	21 ± 8
Automated	14 ± 4	9 ± 3	NA	13 ± 4	26 ± 2	NA
OM1	12	8	17	17	21	19
OM1p5	10	8	18	18	22	18
OM1p5HF	16	10	23	22	28	22
OM1HF	16	10	20	20	25	21

[a]NA, not applicable. Dates are given as mm/yy. Sampling has been performed only manually at Amsterdam Island and Syowa. In parentheses next to the sampling periods and means are the number of paired observations and standard deviations, respectively. The third and forth rows of the mean and standard deviation section are the two-tailed F-test probability (p value) for ($s^2_{Manual}/s^2_{Automated}$), and the 95% confidence interval of the true variance ratio ($\sigma^2_{Manual}/\sigma^2_{Automated}$), respectively. The confidence interval is calculated as ($s^2_{Manual}/s^2_{Automated} \cdot F_{1-\alpha/2,df_{Manual},df_{Automated}} < \sigma^2_{Manual}/\sigma^2_{Automated} < s^2_{Manual}/s^2_{Automated} \cdot F_{\alpha/2,df_{Manual},df_{Automated}}$). The bottom section shows a comparison of observed seasonal cycle (calculated as climatological monthly max Ar/N_2 – monthly min Ar/N_2 ± standard error) to equivalent simulated seasonal cycles.

[b]Agreement is percent of duplicates that differ by more than 16 per meg; the standard deviation of duplicate samples is simply the absolute difference divided by the square root of 2.

presumably due to higher flows at the point of intake [*Blaine et al.*, 2006; *Keeling et al.*, 2004; *Manning*, 2001]. For CGT, MAC, BRW, and SMO, the automated sampler collection was performed at median temperatures and flow rates of −37°C and 5.5 L/min, respectively. Manual sampling at the same stations was performed at median temperatures and flow rates of −66°C and 4 L/min, respectively. Such differences (i.e., higher flow rate) may be responsible for the higher reproducibility in Ar/N_2 measurements. In addition, the reproducibility in sample collection (e.g., duration of purging, valve operation) with the automated systems may also explain the improvement in Ar/N_2 observations.

3.2. Climatological Ar/N_2 Signal

[16] Although a seasonal cycle may not be unambiguous in some of the raw data because of noise in the measurements (Figure 3), a Fourier transform periodogram (auxiliary material Figure S2) clearly shows the predominance of a yearly cycle at all the stations except for Samoa. At the latter station, the seasonal cycle is expected to be small as a result of the small amplitude of the annual temperature cycle in the tropics.

[17] Because of the uncertainty in measurements [*Battle et al.*, 2003] relative to the seasonal Ar/N_2 amplitude (large noise to signal ratio), we average our observations to a climatological year by binning observations in months. The climatological monthly median, which should be less sensitive than the mean to outliers, is not significantly different from the climatological monthly mean. Other algorithms for determining the characteristics of the atmospheric Ar/N_2 seasonal cycle give similar results [*Battle et al.*, 2003]. As in work by *Battle et al.* [2003], we calculate the amplitude of the seasonal cycle at the various stations as (monthly max–monthly min) (Table 1). A clear seasonal cycle is observed in monthly means at each site (Figure 4). During the local summer, Ar/N_2 increases in the atmosphere due to a warming induced degassing of surface waters. As expected, all the Southern Hemisphere stations are in phase, with varying amplitudes. The amplitude of the seasonal cycle is smallest in the tropics (Samoa), and greatest in the Southern Ocean (Macquarie Island).

3.3. Oceanic and Atmospheric Variability in Observations

[18] In addition to measurement errors, the origin of the air collected may introduce variations in Ar/N_2 that could potentially explain some of the observed scatter, including some outliers. Synoptic variability in Ar/N_2 is most likely primarily driven by the atmosphere rather than the ocean [*Battle et al.*, 2003]. Atmospheric transport of Ar/N_2 from various regions could potentially explain the large variability in observations. For example, a wintertime air mass originating south of the Subtropical Front is likely to have a lower Ar/N_2 than an air mass originating from the north because of the tendency for strong heat loss and intermediate water formation to the south, processes that draw Ar and N_2 into the ocean (auxiliary material Figure S3). On the other hand, air that has traveled over land for a significant amount of time is predicted to display a reduced seasonal cycle amplitude due to dilution of the local oceanic Ar/N_2 signal. Similarly, the altitude history of an air mass could also

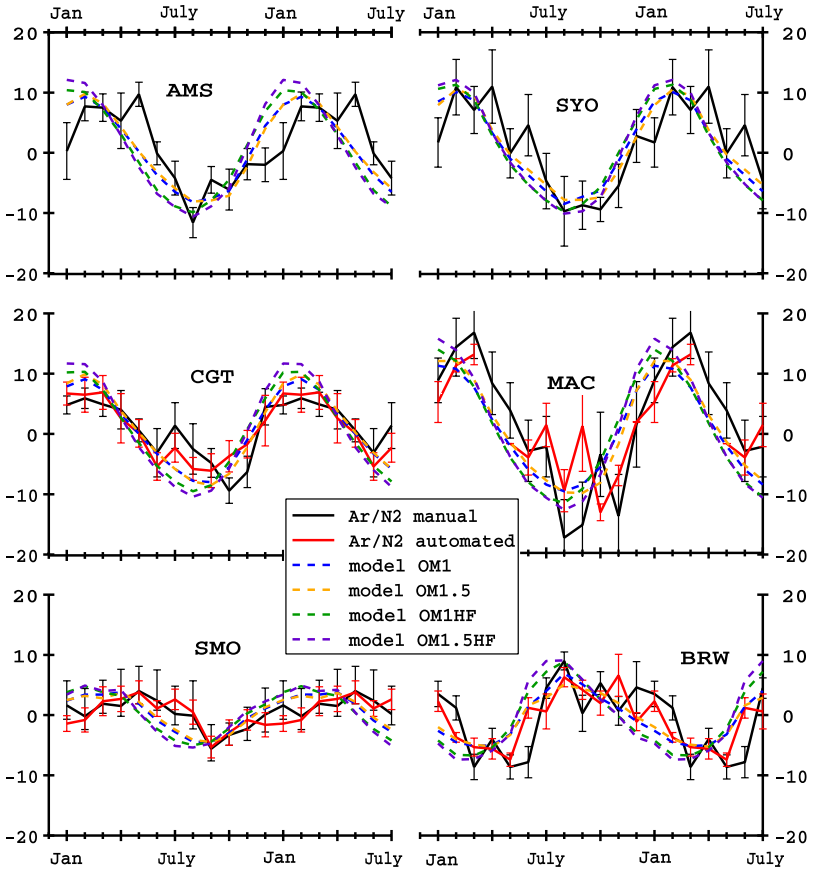

Figure 4. Monthly binned normalized Ar/N_2 climatology and corresponding atmosphere-ocean model predictions over 1.5 climatological years. For each data set, the annual mean Ar/N_2 is set to zero. The black and red lines are spline fits through manual and automated Ar/N_2 collections, respectively. The vertical bars represent the standard error of the climatological monthly means.

have an effect on Ar/N_2 levels because vertical mixing will dilute the local oceanic signal.

[19] Modeling studies give some indication of the characteristic timescale for variability associated with air mass provenance. Analysis of GCTM 6-h results for 2003 illustrates that some of the Ar/N_2 measurement outliers could in fact be due to synoptic atmospheric variability (auxiliary material Figure S4). The standard deviation of the GCTM 6-h model residuals around the mean seasonal cycle climatology (1999–2003) is reflective of the predicted synoptic variability. The standard deviation of the synoptic variability associated with the atmospheric dynamics is predicted to vary from around 1.5 (Samoa) to 2.0 per meg (Macquarie). However, the reproducibility of replicates (Table 1) for automated collection, and the monthly variability in observations (Figure 4) are larger than the synoptic variability in the model. This is evidence that observed variability in Ar/N_2 measurements (Figure 4 and auxiliary material Figure S4) can only be partially accounted for by synoptic variability (see discussion below) and that most of the variability in the observations is analytical.

[20] In order to further explore the variability in Ar/N_2 ratio associated with air mass origin, we investigated the 7 day back trajectories for the samples collected at the various stations between 1998 and 2004 (Figure 5). The back-trajectories were performed using the Hybrid Single-Particle Lagrangian Integrated Trajectory Model (HYSPLIT) (R. R. Draxler and G. D. Rolph, 2003, access via NOAA ARL READY Website, http://www.arl.noaa.gov/ready/hysplit4.html) (also G. D. Rolph, Real-time Environmental Applications and Display sYstem (READY) website, 2003, http://www.arl.noaa.gov/ready/hysplit4.html) and NCEP/NCAR Reanalysis winds for both horizontal and vertical velocities [*Kalnay et al.*, 1996]. Back-trajectories show that, in the case of some stations, the origin of the air collected varies seasonally. For instance, Samoa air preferentially originates from the north in the December to February period, and from further south during June to August (Figure 5 and *Manning et al.* [2003]). Macquarie Island and Cape Grim back-trajectories are relatively homogeneous from season to season, extending from southwest of Australia to the South African sector of the Southern Ocean. The median latitudinal position of the air parcel 7 days prior to sampling is around 75°S to 80°S at Cape Grim, irrespective of the season (albeit slightly further south during the austral fall and summer).

[21] Although the origin of the air is similar at Cape Grim and Macquarie (Figure 5), the observed seasonal amplitudes of Ar/N_2 are significantly greater at Macquarie. Such a difference might conceivably be explained by collection artifacts, such as seasonal changes in thermal fractionation at the air intake [*Blaine et al.*, 2006]. However, the models

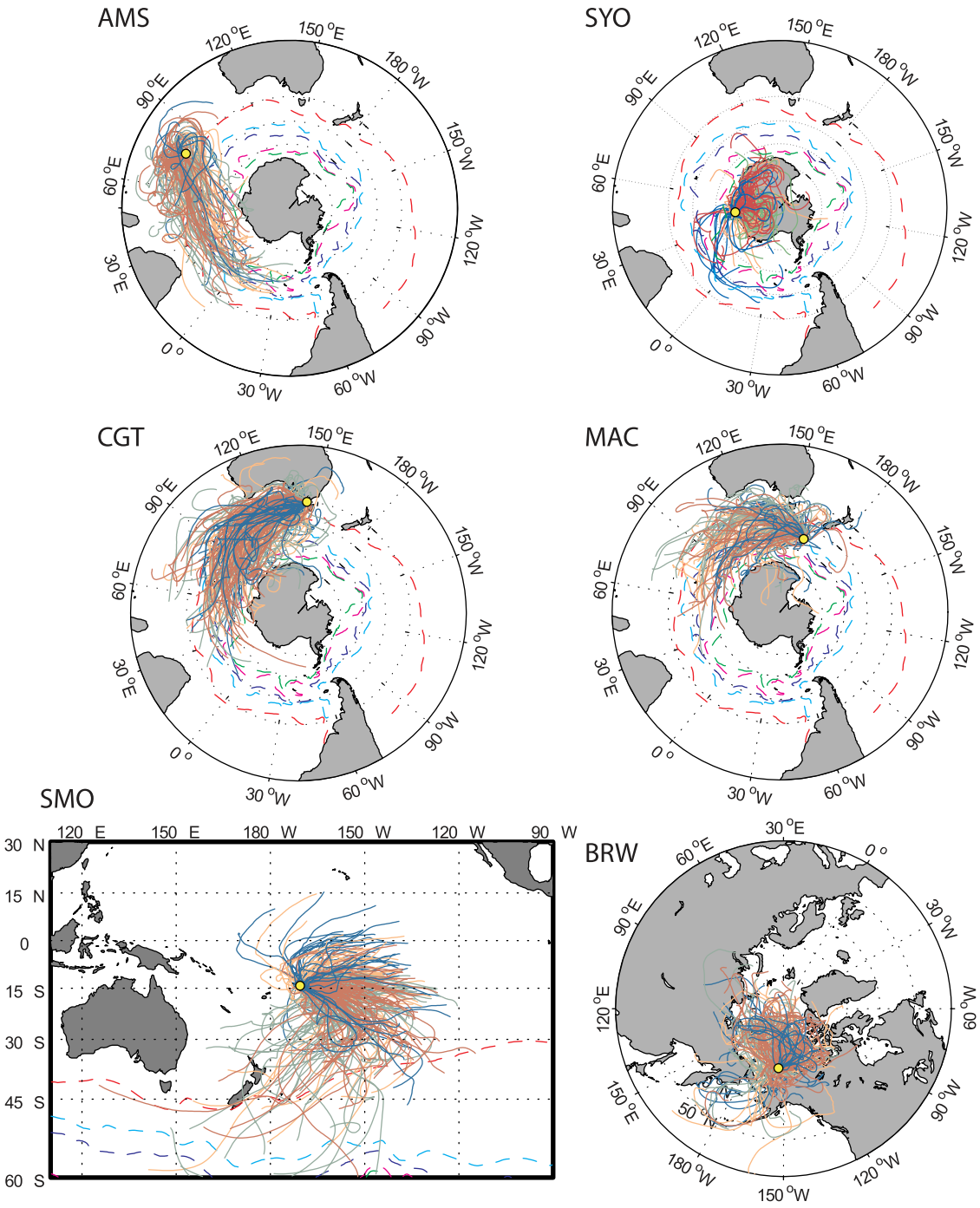

Figure 5. Air parcel back-trajectories for all samples. From left to right and top to bottom: Amsterdam Island, Syowa, Cape Grim, Macquarie Island, Samoa, and Barrow. Stations are represented by yellow circles. Period of the year when sampling occurred is color coded: blue, beige, green, and red for December to February, March to May, June to August, and September to November, respectively. Also depicted in dashed lines are Southern Ocean fronts according to the climatological positions of *Orsi et al.* [1995], from north to south: Subtropical Front, Subantarctic Front, Polar Front, Southern Antarctic Circumpolar Current Front, and the Southern Boundary.

also predict a greater seasonal amplitude at Macquarie than at Cape Grim. The Cape Grim and Macquarie sampling altitudes are 94 m and 12 m above sea level, respectively. The lower altitude of Macquarie back trajectories may explain the larger seasonal cycle relative to Cape Grim. The median altitudes 7 days prior to collection at Macquarie and Cape Grim are 68 and 287 m, respectively. The medians are statistically different (auxiliary material Figure S5). An analysis of the overall altitudes for the 168 h time steps prior to collection also supports that the altitude of sampling at

Macquarie is lower than at Cape Grim. Hence, the Macquarie Island Ar/N_2 signal of ocean processes is less diluted because of the lower altitude of the air mass origin in comparison to Cape Grim. The finding of a substantially larger cycle at Macquarie, dominated by surface layer air parcels, than at Cape Grim, dominated by air parcels from aloft, suggests that Ar/N_2 may be a valuable tracer of the atmospheric rectifier effect [*Denning et al.*, 1995] over the ocean. The rectifier effect is defined as the annual time-mean spatial concentration gradient caused by covariance of atmospheric transport and gas fluxes. The marine boundary layer height is generally assumed to be around 500–1000 m in the Southern Ocean [*Koga and Tanaka*, 1996; *Meskhidze and Nenes*, 2006]. However, it is highly variable and difficult to quantify, particularly over the ocean. The height of the marine boundary layer may vary by a couple of hundred meters over a diurnal cycle [*Wulfmeyer and Janjic*, 2005]. We suspect that, in some cases, the parcel heights along both 7-day trajectories are within the boundary layer, and in others they are above. The fact that a statistically significant difference in the median heights exists, and the fact that there is a pronounced larger seasonal cycle in both data and models at Macquarie suggests that, on average, air masses have been mixed vertically to different extents before arrival at the observing stations.

[22] Back trajectories of outliers (identified, as described earlier by visual inspection and by departures of more than 3 standard deviations from a robust loess fit) have latitude-longitude tracks similar to those of other samplers. However, at Cape Grim, their altitude history is distinct. The median altitude 7 days prior to collection is 287 m for all samples, compared to 14 m for the outliers. It may be that anomalous Ar/N_2 ratios in some of these samples reflect local oceanic fluxes rather than collection artifacts or analysis errors.

3.4. Observations Versus Models' Predictions

[23] As expected, the introduction of Ar and N_2 as active tracers (OM1 and OM1p5) reduces the seasonal Ar/N_2 amplitude and delays the summer maxima and winter minima by about a month relative to the simulations invoking instantaneous equilibration (OM1HF and OM1p5HF) (Figure 4). This difference stems from the lag between the time upper ocean waters acquire or lose heat and the time the resulting gas saturations are relieved by air-sea gas exchange. The slower equilibration time leads to a greater dilution of the Ar/N_2 signal by atmospheric mixing, therefore reducing the modeled seasonal amplitude. Depending on the depth of the mixed layer and wind speed, the residence time of argon and nitrogen is expected to be on the order of 1–2 weeks. Hence, the atmospheric gas signal is expected to lag the heat signal by this amount. We should note that the modeled ocean fluxes for this study are 1-month means. Hence, we cannot at this point capture higher temporal resolution lags in gas exchange (auxiliary material Figure S6).

[24] At most stations, models agree well with observations. As expected, simulations with N_2 and Ar as active tracers are more strongly correlated to observations than simulations that invoke instantaneous equilibration (Figure 4). In Figure 6, we factorially examine the level of agreement between data and models. For each of the four simulations, we calculate the root mean square differences between the monthly mean Ar/N_2 ratio of the data and that of the model. We make this calculation for each of our 6 sites, for each of our 4 models at each site, and 3 data sets: manual collection, automated collection, and all samples. The root mean square residuals reflect discrepancies in the amplitude and phasing between observations and models. In most cases, the automated sampling greatly improves the model fit, even though the automated collection time series represents only 37% (MAC) to 66% (CGT) of the manual collection time series in number of samples, and 28% (MAC) to 90% (CGT) of the duration. With the exception of Cape Grim automated sampling, the highest-resolution model with active Ar and N_2 tracers, OM1p5, outperforms all the other models in agreement to observations (albeit only by a small margin relative to OM1).

[25] The level of agreement between model and observations can be further scrutinized by looking at phasing and amplitude independently. As expected, Ar/N_2 values simulated by the tracer models (OM1 and OM1p5) have a smaller seasonal amplitude than instantaneous equilibration models (OM1HF, and OM1p5HF), and the variations lag slightly. A cross-correlation analysis of observed and simulated Ar/N_2 climatologies confirms that the models' lead over observations has significantly decreased with the inclusion of Ar and N_2 as active tracers relative to heat-derived fluxes at all stations other than Cape Grim (auxiliary material Figure S6). Interestingly, in the case of Cape Grim, all models' predictions (i.e., heat flux and active tracer models) are in phase with observations. This implies that the gas flux for the footprint area of Cape Grim does not significantly lag the heat flux. Although the active tracer models simulate the timing of seasonal variations better than the heat-flux models, the active tracer predictions still slightly lead observations with the exception of Cape Grim.

[26] Overall, the OM1 and OM1p5 seasonal amplitude predictions are within the error bounds of observations (more specifically observations collected automatically), except at Macquarie Island. At Macquarie, the Ar/N_2 seasonal amplitude by automated sampling agrees better with model predictions than manual sampling observations. However, OM1HF and OM1p5HF predictions are more in line with the observed seasonal cycle amplitude than the active tracer models. This occurs despite the fact that the heat flux approach should overestimate the amplitude of the seasonal cycle, a fact confirmed by the model-data comparisons at the other locations. We also note that Macquarie is more predominantly influenced by air parcels from the boundary layer (section 3). Together, this suggests that GCTM may have too much mixing out of the boundary layer over the ocean upwind of the island [*Denning et al.*, 1995].

[27] *Battle et al.* [2003] used two atmospheric transport models and two ocean heat flux estimates for calculating Ar and N_2 air-sea fluxes. They calculated Ar/N_2 time curves for 3 possible combinations of ocean heat flux and atmospheric transport. Each pairing of the above agreed with another pairing at one or more locations, but never at all locations. This result shows that compensating impacts on atmospheric Ar and N_2 concentrations can occur in the atmo-

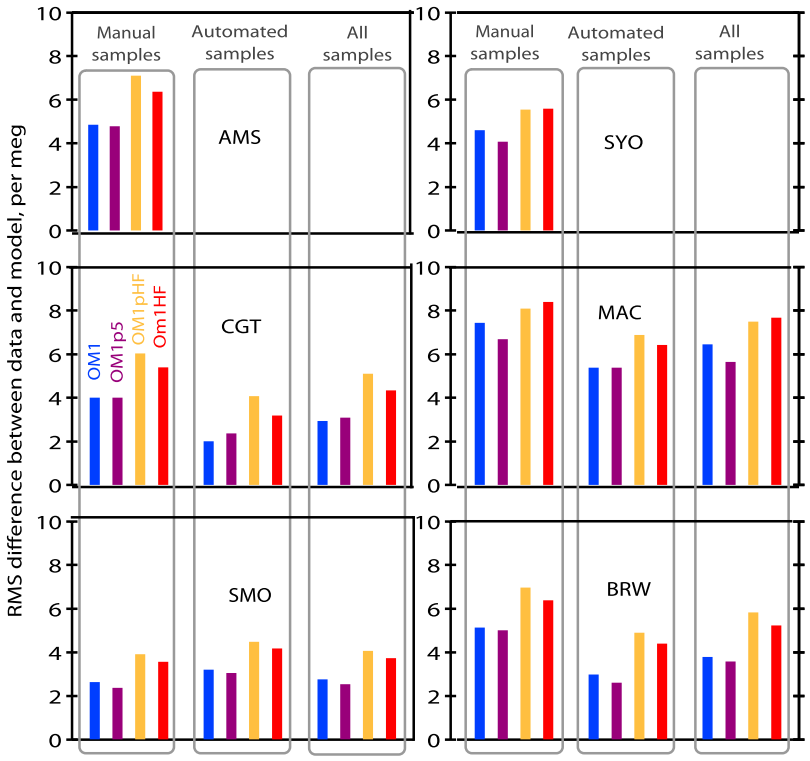

Figure 6. Root mean square differences between climatological monthly means of models and observations at our six sampling sites. Stations AMS and SYO only have manual sampling results. OM1, OM1p5, OM1p5HF, and OM1HF are in blue, purple, yellow, and red, respectively. Models OM1 and OM1p5 invoke gas transfer according to mixed layer supersaturation and piston velocity, whereas OM1HF and OM1p5HF invoke instantaneous air-sea equilibration.

spheric and ocean models. It also demonstrates that ocean model flux estimates and atmospheric transport estimates likely have uncertainties of comparable magnitudes. In-depth evaluation of the paired modeling system will become possible only as the Ar/N_2 record increases in length and reduces in noise to signal ratio.

4. Conclusion

[28] We have presented a new climatology for Ar/N_2 variations based on longer data sets and improved methods of sample collection. The introduction of automated samplers has significantly reduced the errors associated with air collection. Thermal fractionation could however still be significant [*Keeling et al.*, 2004]. We have also made new simulations of atmospheric Ar/N_2 variations improved by invoking kinetically regulated gas exchange at the air-sea interface.

[29] With the more realistic gas exchange rate model predictions, longer time series, and improvement in Ar/N_2 measurements by automated sampling, agreement between data and models is now better than in a previous study by *Battle et al.* [2003]. Our results also suggest that air parcel history may partially explain some of the variability in Ar/N_2 measurements at a given station and between stations. The paired models are, to first order, accurately estimating air-sea heat and gas fluxes. Despite these improvements, the noise to signal ratio in our Ar/N_2 time series is still too large to make further progress in evaluating model simulations with respect to interannual variability, latitudinal gradients and a secular increase in Ar/N_2 due to ocean warming.

[30] **Acknowledgments.** We thank Roland Draxler (NOAA), Arlene Fiore, Songmiao Fan, and Bud Moxim (GFDL) for helpful discussions and assistance with GCTM. We thank Roberta Hamme for sharing her oceanic Ar and N_2 measurements and Dierk Polzin for assistance with figures. We are grateful to the scientists at the various atmospheric stations who have carefully collected the air samples and whom have made this research possible. We also gratefully acknowledge the NOAA Air Resources Laboratory (ARL) for the provision of the HYSPLIT transport and dispersion model and READY website (http://www.arl.noaa.gov/ready.html) used in this publication. This research was supported by the BP-Amoco-Princeton Carbon Mitigation Initiative and grants from the National Science Foundation and the National Oceanic and Atmospheric Administration, and the Anna Julia Cooper Postdoctoral Fellowship from University of Wisconsin-Madison (GAM).

References

Battle, M., M. Bender, M. B. Hendricks, D. T. Ho, R. Mika, G. McKinley, S. Fan, T. Blaine, and R. F. Keeling (2003), Measurements and models of the atmospheric Ar/N_2 ratio, *Geophys. Res. Lett.*, *30*(15), 1786, doi:10.1029/2003GL017411.

Bender, M. L., D. T. Ho, M. B. Hendricks, R. Mika, M. O. Battle, P. P. Tans, T. J. Conway, B. Sturtevant, and N. Cassar (2005), Atmospheric O_2/N_2 changes, 1993–2002: Implications for the partitioning of fossil fuel CO_2 sequestration, *Global Biogeochem. Cycles*, *19*, GB4017, doi:10.1029/2004GB002410.

Blaine, T. W., R. F. Keeling, and W. J. Paplawsky (2006), An improved inlet for precisely measuring the atmospheric Ar/N_2 ratio, *Atmos. Chem. Phys.*, *6*, 1181–1184.

Cleveland, W. S. (1979), Robust locally weighted regression and smoothing scatterplots, *J. Am. Stat. Assoc.*, *74*, 829–836, doi:10.2307/2286407.

Cleveland, W. S., and S. J. Devlin (1988), Locally weighted regression: An approach to regression analysis by local fitting, *J. Am. Stat. Assoc.*, *83*, 596–610.

Denning, A. S., I. Y. Fung, and D. Randall (1995), Latitudinal gradient of atmospheric CO_2 due to seasonal exchange with land biota, *Nature*, *376*, 240–243, doi:10.1038/376240a0.

Fan, S. M., L. W. Horowitz, H. Levy II, and W. J. Moxim (2004), Impact of air pollution on wet deposition of mineral dust aerosols, *Geophys. Res. Lett.*, *31*, L02104, doi:10.1029/2003GL018501.

Ganachaud, A., and C. Wunsch (2000), Improved estimates of global ocean circulation, heat transport and mixing from hydrographic data, *Nature*, *408*, 453–457, doi:10.1038/35044048.

Griffies, S. M., M. J. Harrison, R. C. Pacanowski, and A. Rosati (2004), A technical guide to MOM4, *Tech. Rep. 5*, Ocean Group, Geophys. Fluid Dyn. Lab., Princeton, N. J.

Kalnay, E., et al. (1996), The NCEP/NCAR 40-year reanalysis project, *Bull. Am. Meteorol. Soc.*, *77*, 437–471, doi:10.1175/1520-0477(1996)077<0437:TNYRP>2.0.CO;2.

Keeling, R. F., T. Blaine, B. Paplawsky, L. Katz, C. Atwood, and T. Brockwell (2004), Measurement of changes in atmospheric Ar/N_2 ratio using a rapid-switching, single-capillary mass spectrometer system, *Tellus, Ser. B*, *56*, 322–338, doi:10.1111/j.1600-0889.2004.00117.x.

Koga, S., and H. Tanaka (1996), Simulations of seasonal variations of sulfur compounds in the remote marine atmosphere, *J. Atmos. Chem.*, *23*, 163–192, doi:10.1007/BF00048259.

Levitus, S., J. I. Antonov, T. P. Boyer, and C. Stephens (2000), Warming of the world ocean, *Science*, *287*, 2225–2229, doi:10.1126/science.287.5461.2225.

Levitus, S., J. Antonov, and T. Boyer (2005), Warming of the world ocean, 1955–2003, *Geophys. Res. Lett.*, *32*, L02604, doi:10.1029/2004GL021592.

Mahlman, J. D., and W. J. Moxim (1978), Tracer simulation using a global general circulation model: Results from a mid-latitude instantaneous source experiment, *J. Atmos. Sci.*, *35*, 1340–1374, doi:10.1175/1520-0469(1978)035<1340:TSUAGG>2.0.CO;2.

Manning, A. C., (2001), Temporal variability of atmospheric oxygen from both continuous measurements and a flask sampling network: Tools for studying the global carbon cycle, Ph.D. thesis, Univ. of Calif., San Diego.

Manning, A. C., R. F. Keeling, L. E. Katz, W. J. Paplawsky, and E. M. McEvoy (2003), Interpreting the seasonal cycles of atmospheric oxygen and carbon dioxide concentrations at American Samoa Observatory, *Geophys. Res. Lett.*, *30*(6), 1333, doi:10.1029/2001GL014312.

McKinley, G. A. (2004), Testing ocean models with argon and nitrogen, *Eos Trans. AGU*, *85*(47), Fall Meet. Suppl., Abstract OS13B–0526.

Meskhidze, N., and A. Nenes (2006), Phytoplankton and cloudiness in the Southern Ocean, *Science*, *314*, 1419–1423, doi:10.1126/science.1131779.

Neubert, R. E. M., L. L. Spijkervet, J. K. Schut, H. A. Been, and H. A. J. Meijer (2004), A computer-controlled continuous air drying and flask sampling system, *J. Atmos. Oceanic Technol.*, *21*, 651–659, doi:10.1175/1520-0426(2004)021<0651:ACCADA>2.0.CO;2.

Orr, J. C., et al. (2001), Estimates of anthropogenic carbon uptake from four three-dimensional global ocean models, *Global Biogeochem. Cycles*, *15*, 43–60, doi:10.1029/2000GB001273.

Orsi, A. H., T. Whitworth, and W. D. Nowlin (1995), On the meridional extent and fronts of the Antarctic Circumpolar Current, *Deep Sea Res., Part I*, *42*, 641–673, doi:10.1016/0967-0637(95)00021-W.

Stephens, B. B., P. S. Bakwin, P. P. Tans, R. M. Teclaw, and D. D. Baumann (2007), Application of a differential fuel-cell analyzer for measuring atmospheric oxygen variations, *J. Atmos. Oceanic Technol.*, *24*, 82–94, doi:10.1175/JTECH1959.1.

Wanninkhof, R. (1992), Relationship between wind-speed and gas-exchange over the ocean, *J. Geophys. Res.*, *97*, 7373–7382, doi:10.1029/92JC00188.

Wulfmeyer, V., and T. Janjic (2005), Twenty-four-hour observations of the marine boundary layer using shipborne NOAA high-resolution Doppler lidar, *J. Appl. Meteorol.*, *44*, 1723–1744, doi:10.1175/JAM2296.1.

M. Battle, Department of Physics and Astronomy, Bowdoin College, Brunswick, ME 04011, USA.

M. L. Bender, N. Cassar, and R. Mika, Department of Geosciences, Princeton University, 1000 Pope Road, Princeton, NJ 08544, USA. (ncassar@princeton.edu)

G. A. McKinley, Department of Atmospheric and Oceanic Sciences, University of Wisconsin-Madison, Madison, WI 53706, USA.